Long-range organization of primary intestinal fibroblasts guides directed and persistent migration of organoid-derived intestinal epithelia

Vanesa Fernández-Majada[1#*], Jordi Comelles[1,2#], Aina Abad-Lázaro[1#], Verónica Acevedo[1], Anna Esteve-Codina[3], Xavier Hernando-Momblona[4,5], Eduard Batlle[4,5,6], Elena Martinez[1,2,7*]

[1] *Biomimetic Systems for Cell Engineering Laboratory, Institute for Bioengineering of Catalonia (IBEC), The Barcelona Institute of Science and Technology (BIST), Baldiri Reixac 15-21, 08028 Barcelona, Spain*

[2] *Department of Electronics and Biomedical Engineering, University of Barcelona (UB), Martí i Franquès 1, 08028 Barcelona, Spain*

[3] *Centre Nacional d'Anàlisi Genòmica – Centre de Regulació Genòmica (CNAG-CRG) Barcelona Science Park - Tower I. Baldiri Reixac, 4. 08028 Barcelona*

[4] *Colorectal Cancer Laboratory, Institute for Research in Biomedicine (IRB Barcelona), The Barcelona Institute of Science and Technology (BIST), Baldiri Reixac 10-12, 08028 Barcelona, Spain*

[5] *Centro de Investigación Biomédica en Red (CIBERONC), Barcelona, Spain.*

[6] *ICREA, Passeig Lluís Companys 23, 08010 Barcelona, Spain.*

[7] *Centro de Investigación Biomédica en Red (CIBER), Av. Monforte de Lemos 3-5, Pabellón 11, Planta 0, 28029 Madrid, Spain*

[#]These authors contributed to this work equally

*Sharing corresponding authorship. Contact information:

Biomimetic Systems for Cell Engineering Laboratory, Institute for Bioengineering of Catalonia (IBEC), Baldiri Reixac, 15-21, 08028 Barcelona, Spain

E-mail address: emartinez@ibecbarcelona.eu; vfernandez@ibecbarcelona.eu

Tel: +34 934 037 177

Fax: +34 934 034 750

Abstract

Fibroblasts reside underneath most epithelial tissues. In the intestine, their role has been mostly restricted to a secretory and supportive role. Recent studies have shown that fibroblasts' migration is key during vilification and wound healing. Yet, whether interactions between epithelial cells with fibroblasts and with the matrix contribute to epithelial movement remains elusive. Here, we show that intestinal fibroblasts enhance the directed and persistent migration of organoid-derived intestinal epithelia. By using a novel gap closure *in vitro* model of the intestinal mucosa that includes both the epithelium and the stromal compartments, we demonstrate that the physical presence of fibroblasts in contact with the epithelium plays a crucial role in epithelial restoration by enhancing epithelial tissue integrity. Our results demonstrate that fibroblasts undergo long-range ordering to align perpendicularly to the epithelial migrating front, and deposit protein paths that act as contact guidance features to direct epithelial migration. In turn, only the physical interaction of intestinal fibroblasts with intestinal organoids drives epithelial spreading in three dimensions. Our results demonstrate that fibroblasts actively coordinate to accelerate intestinal epithelial restoration.

Introduction

Fibroblasts line underneath epithelial layers in most organs. They constitute the primary component of a supportive mesenchymal compartment that interfaces with epithelial cells via a basement membrane primarily composed of laminin and type IV collagen.[1] Beyond providing physical support, subepithelial fibroblasts play a crucial role in regulating various epithelial processes throughout development, homeostasis, and disease. For instance, they restrain duct elongation and control branching in mammary glands,[2] and regulate bronchial epithelial repair during lung inflammation or injury[3]. Also, analyses carried out in skin,[4] cornea,[5,6] or cleaved palate,[7] indicate that fibroblasts contribute to epithelial restoration upon injury.[8,9] Thus, understanding the complex interplay between fibroblasts and epithelia across different

contexts and how they mechanistically integrate for tissue function, is a fundamental question. This has broad implications for tissue engineering, developmental biology, and regenerative medicine, offering insights into both physiological maintenance and pathological conditions.

In the intestinal tract, the epithelial layer is also supported by fibroblasts present in the lamina propria.[10–13] The different subpopulations of these intestinal fibroblasts vary in morphology, secretory profile and localization along the crypt-villus axis that compartmentalizes the intestinal epithelium.[14] They are known to play a crucial role in maintaining epithelial homeostasis by secreting various factors[15,16] including Wnts,[17] R-spondins,[16,18] Bone Morphogenetic Protein (BMP) agonists and antagonists,[14,19–21] as well as Epidermal Growth Factor Receptor (EGFR) ligands.[22] However, their role is not solely restricted to provide paracrine signaling but they also physically interact with epithelial cells. For example, migration and aggregation of Platelet Derived Growth Factor Receptor A $(PDGFRA)^{+}$ subepithelial fibroblasts seems sufficient for generating the curvature needed to drive villi formation during intestinal development in mice.[23]

Moreover, *in vivo* wound healing experiments in colonic epithelium have underscored the significance of both the epithelial and mesenchymal components in tissue repair.[24–27] The epithelial integrity hinges on the migration of non-proliferative wound-associated epithelial (WAE) cells, originating from crypts adjacent to the wound and moving over the wound surface.[24] The differentiation of these specialized WAE cells is regulated by the signaling of fibroblasts localized at the site of injury producing Prostaglandin E2 (PGE2).[26,27] However, there is still limited understanding regarding the early migration of intestinal epithelial cells following injury. In particular, it remains unclear whether and how the physical interaction between these cells and intestinal fibroblasts influences epithelial migration and function restoration beyond fibroblasts' secretory function.

Early *in vitro* studies have shown that intestinal epithelial Caco-2 cells close wounds more effectively when cultured on intestinal myofibroblasts compared to when cultured on extracellular matrix (ECM)-coated plastic plates.[28] However, this cell line does not accurately replicate the unique migratory dynamics of the in vivo intestine, and the mechanisms behind fibroblast-mediated migration are not well understood. Recently, intestinal and colon organoids have been successfully opened-up into 2D monolayers.[29,30] These monolayers retrieve all the *in vivo* cell populations and their organization in crypt and villus-like compartments, facilitating the study of signaling feedback loops and mechanical patterning and migration,

for instance.[29,31] Despite this progress, the role of the stromal compartment has been largely overlooked. Here, by using a novel intestinal mucosa model that includes organoid-derived intestinal epithelial cells, primary intestinal fibroblasts, and a basement membrane matrix, we provide evidence that the physical interaction between intestinal fibroblasts and epithelia induces a long-range organization of fibroblasts, which, in its turn, results in a directed and persistent migration of epithelial cells leading to the restoration of intestinal epithelial tissue in an *in vitro* gap closure model.

The presence of fibroblasts underneath organoid-derived intestinal epithelium enhances its restoration

To investigate the role of the physical crosstalk between Intestinal Epithelial Cells (IECs) and intestinal fibroblasts, we set up a physiological-like model of intestinal mucosa *in vitro* (Figure 1a). This model included primary mouse fibroblasts and organoid-derived intestinal mouse epithelial cells, which grew as self-organized monolayers following an in-house developed protocol.[30,32]

Primary fibroblasts were extracted from mouse intestinal mucosa and meticulously analyzed using single-cell RNA sequencing (scRNAseq) [see supplementary material]. The predominant population, comprising roughly 75% of the total cells, displayed Vimentin expression, confirming their fibroblast nature (Figure 1b). These fibroblasts were further delineated into clusters expressing key factors associated with Wnt and BMP signaling pathways, suggesting their potential involvement in facilitating epithelial cell proliferation and differentiation. Importantly, the transcriptomic profile of these fibroblasts closely mirrored known fibroblastic populations adjacent to the intestinal epithelium.[14]

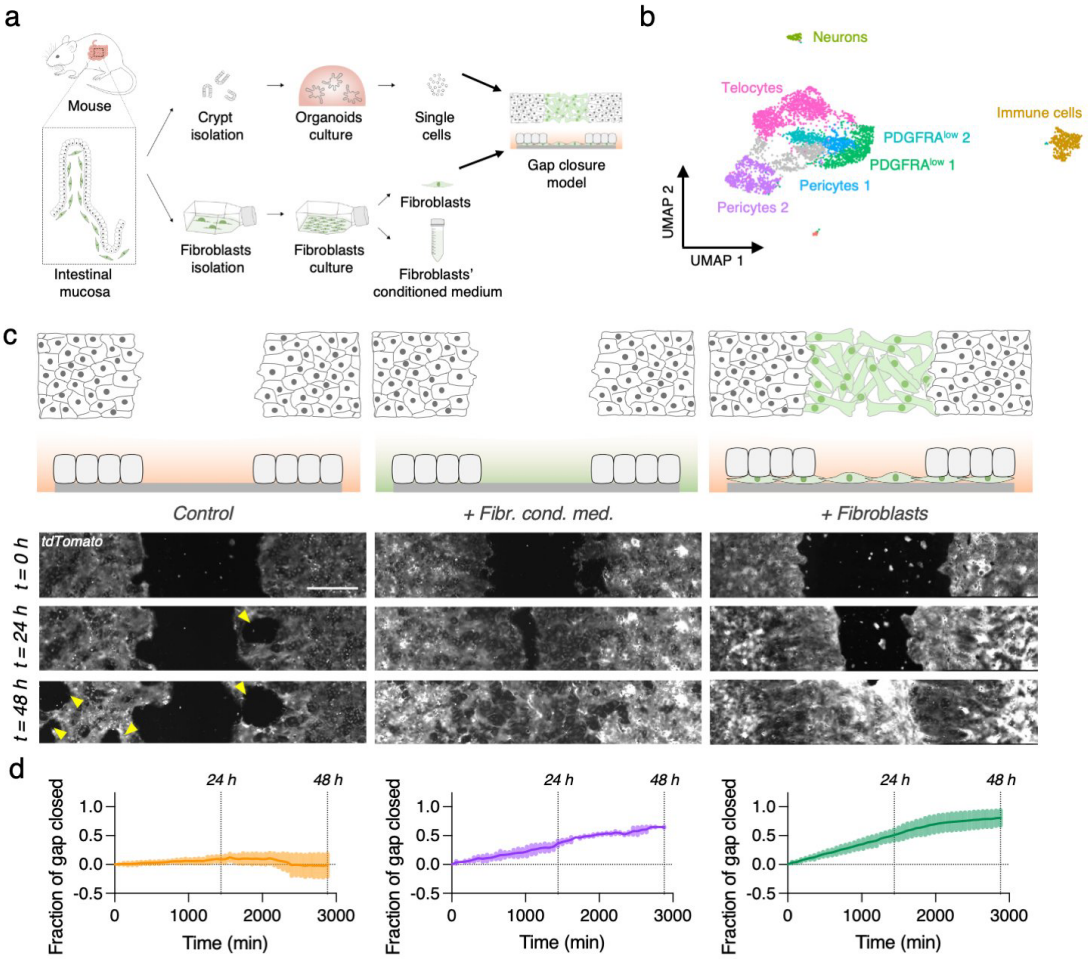

Figure 1. (a) Schematics of the experimental set-up. (b) Uniform manifold approximation and projection (UMAP) of established primary culture from small intestine stroma. Resident populations were dominated by molecularly distinct clusters of telocytes, pericytes and PDGFRA^{low} cells. Grey dots represent cells that could not be integrated within a cluster. (c) Schematics of the experimental set-up (top). Snapshots of the live-imaging of tdTomato organoid-derived cells migrating in control, + fibr. cond. med. and + fibroblasts conditions at 0, 24 and 48h upon barrier removal (bottom). Yellow arrows highlight holes in the monolayers. Scale bar: 500 µm. (d) Fraction of gap closed along time in control, + fibr. cond. med. and + fibroblasts conditions. Mean ± SEM.

First, we grew a monolayer of these intestinal fibroblasts on a thin layer of Matrigel. Then, we placed customized elastomeric barriers on top of this monolayer. Subsequently, we seeded IECs derived from *Lgr5-EGFP/RCL-tdT* organoids on top the fibroblasts. After the formation of the epithelial monolayer, we removed the elastomeric barrier creating an epithelium-free gap, and we proceeded to observe and track

for 48 hours the migration of epithelial cells attempting to close the gap (+ fibroblasts condition). To unravel the potential role of fibroblasts in this gap closure process, we tested two additional gap conditions: (i) epithelial cells alone (control), and (ii) epithelial cells cultured with fibroblasts' conditioned medium (+ fibr. cond. med.) (Figure 1c). Right after the removal of the elastomeric barrier, all conditions displayed confluent epithelial monolayers with crypt-like and villus-like compartmentalization,[29–31] independently on the presence of the fibroblasts or their conditioned medium (Figure 1c, t = 0 hours, Figure S2a-d). However, after 24 hours, noticeable differences emerged among the conditions. In the + fibr. cond. med. and + fibroblasts conditions, the epithelial front advanced, resulting in significant gap closure. In contrast, the controls exhibited poor epithelial movement and a disruption in the epithelial cohesion, as seen by the emergence of holes within the monolayers (Movie 1 and Figure 1c, t = 24 hours, indicated by yellow arrow). After 48 hours, gap closure failed for the control monolayers, and the number and size of holes within the tissue had significantly increased (Figure 1c, t = 48 hours, indicated by yellow arrows). Meanwhile, the + fibr. cond. med. and + fibroblasts conditions succeeded in closing the gap. Actually, epithelial monolayers achieved the most effective gap closure when cultured in direct physical contact with the fibroblasts (Figure 1d and Movies 2 and 3).

Differences in gap closure do not depend on cell proliferation

Intestinal epithelial migration has been traditionally explained by the mitotic pressure arising from cell proliferation within the crypts.[33,34] To elucidate whether the physical presence of fibroblasts has a substantial role in epithelial proliferation during gap closure, we used the proliferation marker Ki-67 to quantify the percentage of proliferative cells both within the monolayer regions and at the leading edge of epithelial migration (Figure S3). Within the monolayers, proliferative cells accounted approximately for 5% of the population and were found in clusters, typically linked to crypt-like domains (Figure S2d)[29–31] for all the three gap closure conditions tested. However, at the migration front, the population of Ki-67^{+} cells was significantly enlarged and accounted for more than 20% for all experimental conditions (Figure S3). On the other hand, the number of cells positive for the apoptotic marker Cleaved Caspase-3 (CC3) was lower and similar in all three conditions (Figure S3). Therefore, the similarities in cell proliferation and death among the three experimental conditions do not provide an explanation for the differences observed in gap closure.

These differences then could be related to how fibroblasts impact the integrity and the migration of the epithelial monolayer.

Fibroblasts trigger the directed and persistent migration of organoid-derived intestinal epithelial cells for effective gap restoration

To gain further insights into the differences observed in gap restoration for the three conditions, we analyzed individual cell trajectories. In the control, intestinal epithelial cells (IECs) trajectories were poorly oriented towards the gap (Figure 2a, b). This was mostly caused by the formation of enduring holes in the epithelia (Figure S4a and movie 4). In contrast, IECs trajectories were better oriented towards the gap in the + fibr. cond. med. condition and completely oriented in the + fibroblasts condition (Figure 2a,b). Interestingly, time-lapse experiments revealed that tissue holes were also formed in these conditions, but they were quickly and successfully closed, thus rapidly restoring the monolayer integrity (Figure S4a-c and movie 5 and 6).

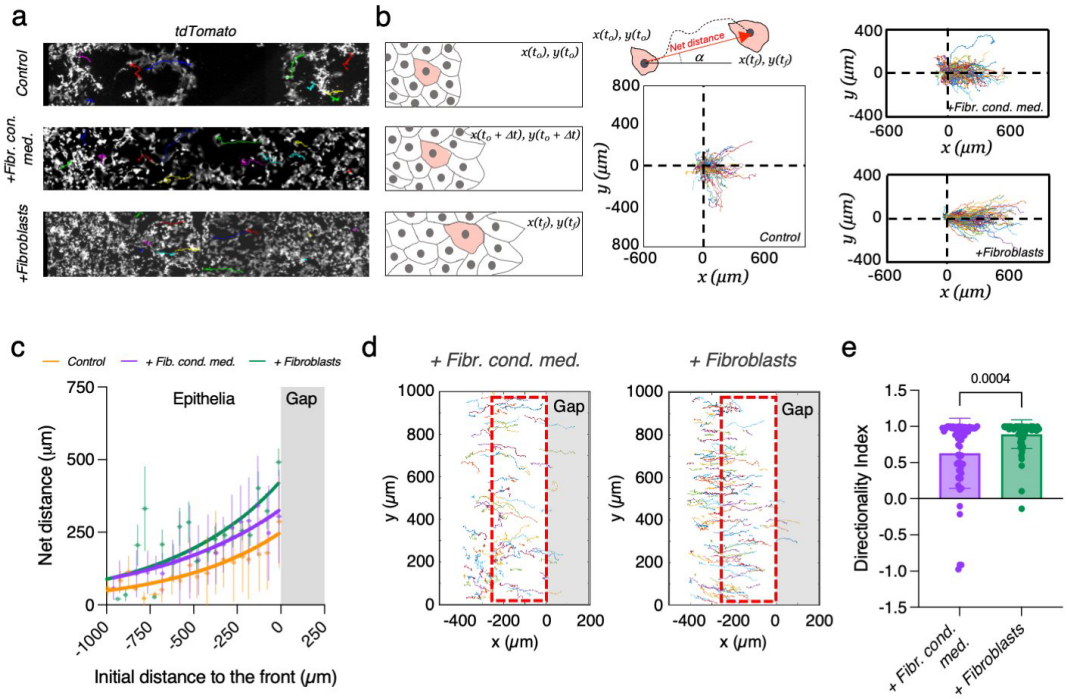

Figure 2. (a) Individual cell trajectories for each of the culture conditions. (b) Schematics of the tracking analysis and the net displacement vector. Trajectories of each individual cell centered at the origin at t = 0. The direction of the gap is at x > 0. (c) Net displacement as a function of the initial distance to the migration front for each culture condition. Dots represent the mean value ± SEM, the solid line corresponds to an exponential fitting. The gray region corresponds

to the gap. (d) Cell trajectories for the different experimental conditions. The gray region corresponds to the gap while the red rectangle highlights the first 250 μm of the epithelium behind the migration front. (e) Directionality index for cells' trajectories within the first 250 μm behind the migration front. Mean ± SD and individual values. Kruskal-Wallis test.

Next, for each cell trajectory we further measured: (i) the net displacement, (ii), the total distance traveled and (iii) the directionality index with respect to the gap for each trajectory (Figure 2b, c, and Figure S5). Compared to the control condition, the average net displacement was increased in response to fibroblasts input, whether paracrine or physical (Figure 2c). In addition, we found that paracrine signaling induced a progressive increase in the cell net displacement for cells closer to the migration front (gray stripe in the graph of Figure 2d). This increase was further enhanced when fibroblasts were physically present. Thus, net cell displacements depended on their position within the epithelium and differed between cells exposed only to paracrine signals and those with also the physical presence of intestinal fibroblasts (Figure 2c), leading to higher persistent cell motion.

When examining the cell trajectories near the gap, they appeared straighter and more aligned when fibroblasts were physically present, compared to when they were in the condition with fibroblast-conditioned medium (Figure 2d). To quantify this observation, we defined the alignment index ($\cos(2\cdot\alpha)$), which equals 1 when the net displacement is in the direction of the gap and -1 when it is perpendicular. Plotting $\cos(2\cdot\alpha)$ as a function of the distance to the migration front (Figure S5b), we observed that in the control condition, epithelial cells showed no alignment across the monolayer. In contrast, when cultured with fibroblasts-conditioned medium, trajectories became more aligned to the gap direction, particularly those closer to the migration front. This tendency was significantly enhanced when fibroblasts were present, resulting in trajectories with $\cos(2\cdot\alpha)$ close to 1, specially within the first 250 μm closer to the migration front (Figure 2e). Overall, these results show a higher persistent and directional migration of the epithelial cells when intestinal fibroblasts are in the culture, compared to paracrine signal alone. This points toward the existence of physical interactions between the IECs and the fibroblasts that collaborate to regulate epithelial migration.

Primary fibroblasts at the gap favor an efficient epithelial migration

To further investigate this physical interaction between the epithelial cells and the fibroblasts, we designed an additional experimental setup. We compared epithelial cell migration on an intact monolayer of fibroblasts (+ fibroblasts condition) with a scenario where the fibroblast monolayer was interrupted in the gap region (empty gap condition, Figure 3a). To create this setup, we first placed the elastomeric barrier on the substrate and then seeded primary fibroblasts, spatially confining them to both sides of the barrier. Once the fibroblasts had formed a monolayer, we seeded the IECs until they also formed monolayer and we removed the barrier, creating a gap empty of fibroblasts. Both cell types started migrating towards the gap simultaneously (Movie 7), but, on average, epithelial cells reached a lower fraction of gap closure when compared to when fibroblasts were present in the gap (+ fibroblasts condition) (Figures 3b, 3c and Movie 7). Moreover, net distances were shorter, and the alignment of the trajectories was reduced when the gap was initially devoid of fibroblasts, thus leading to a less persistent and directed migration (Figure 3d and e). These findings collectively imply that maintaining an intact fibroblast monolayer, rather than solely having fibroblasts beneath the epithelia, leads to more efficient epithelial migration and gap closure. Furthermore, it suggests that fibroblasts located far from the epithelial front may significantly contribute to the efficiency of epithelial cell migration.

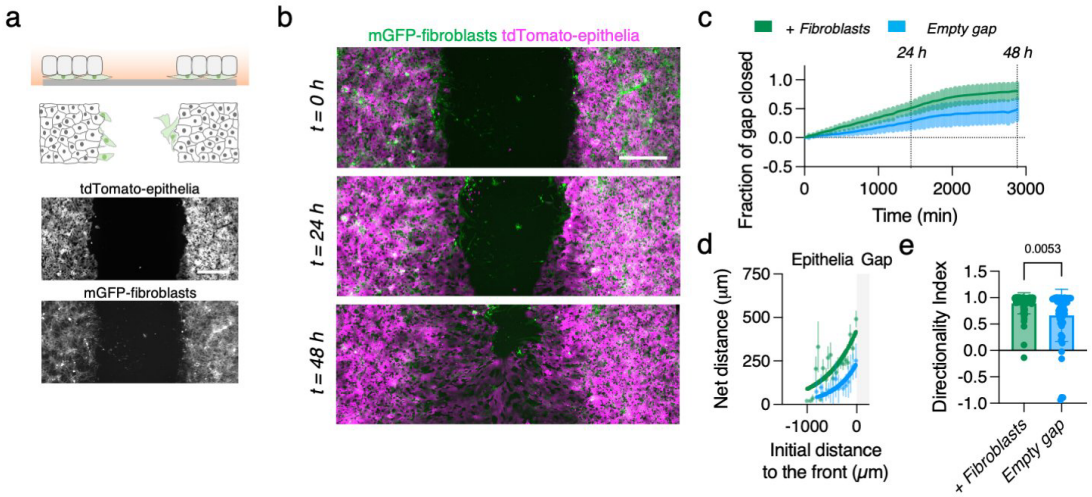

Figure 3. (a) Schematics of the experimental set-up of the “empty gap” condition. Scale bar: 500 μm. (b) Sum intensity projections of timeframes corresponding to 0, 24 and 48h upon barrier removal of the empty gap condition. Scale bar: 500 μm. (c) Fraction of gap closed over time. Mean ± SEM. (d) Net displacement as a function of the initial distance to the migration front. Dots represent the mean value, and bars the SEM, the solid line corresponds to an exponential

fitting. Gray region corresponds to the gap outside the epithelium. (e) Directionality index for cells' trajectories within the first 250 μm behind the migration front. Mean + SD and individual values.

Fibroblasts activate and migrate towards the epithelial front

Results above point toward the existence of physical interactions between the IEC and the fibroblasts that collaborate to regulate epithelial migration, not only from that underneath the epithelia but also from those further away inside the gap. To better understand these interactions, we studied more in detail the gap closure process in the +fibroblasts condition. First, we stained the gap region at various time points to examine the epithelial front and the distribution of fibroblasts close to it (Figure 4a). Upon removal of the barrier (t = 0 h), fibroblasts at the epithelial front were small and evenly distributed, with no prominent α-SMA fibers present. However, 24 and 48 hours after barrier removal, fibroblasts were more abundant and appeared bigger and activated, exhibiting prominent α-SMA fibers, both beneath the epithelial front and within the gap region closer to the leading edge. Then, we analyzed the onset of gap closure (first 9 hours after removing the barrier) using particle image velocimetry (PIV), which allowed us to obtain velocity fields from both the IECs and the fibroblasts. Strikingly, two clearly differentiated regions appeared on the maps of the x-component of the cells' mean velocities (v_x) (Figure 4b). IECs exhibited on average $v_x > 0$, so they were migrating toward the gap. In contrast, fibroblasts displayed on average $v_x < 0$, indicating that they were migrating from the gap toward the epithelium. The temporal evolution of the x-component of the instantaneous velocity revealed the expansion of the $v_x > 0$ region toward the gap, which correlated with the advancing epithelium (Figure 4c). Furthermore, the averaged velocity profiles of the x-component (v_x) and the y-component (v_y) across the migration fronts and adjacent gap regions indicated that migration occurred mainly in the direction perpendicular to the front for both cell types and that fibroblasts in the gap region actively moved toward the front of the migrating epithelium ($v_x < 0$, $v_y \sim 0$) (Figure 4d). Altogether, upon barrier removal fibroblasts migrate from the gap towards the leading edge of the epithelia, where they express prominent α-SMA fibers and seem to interact with the epithelial cells.

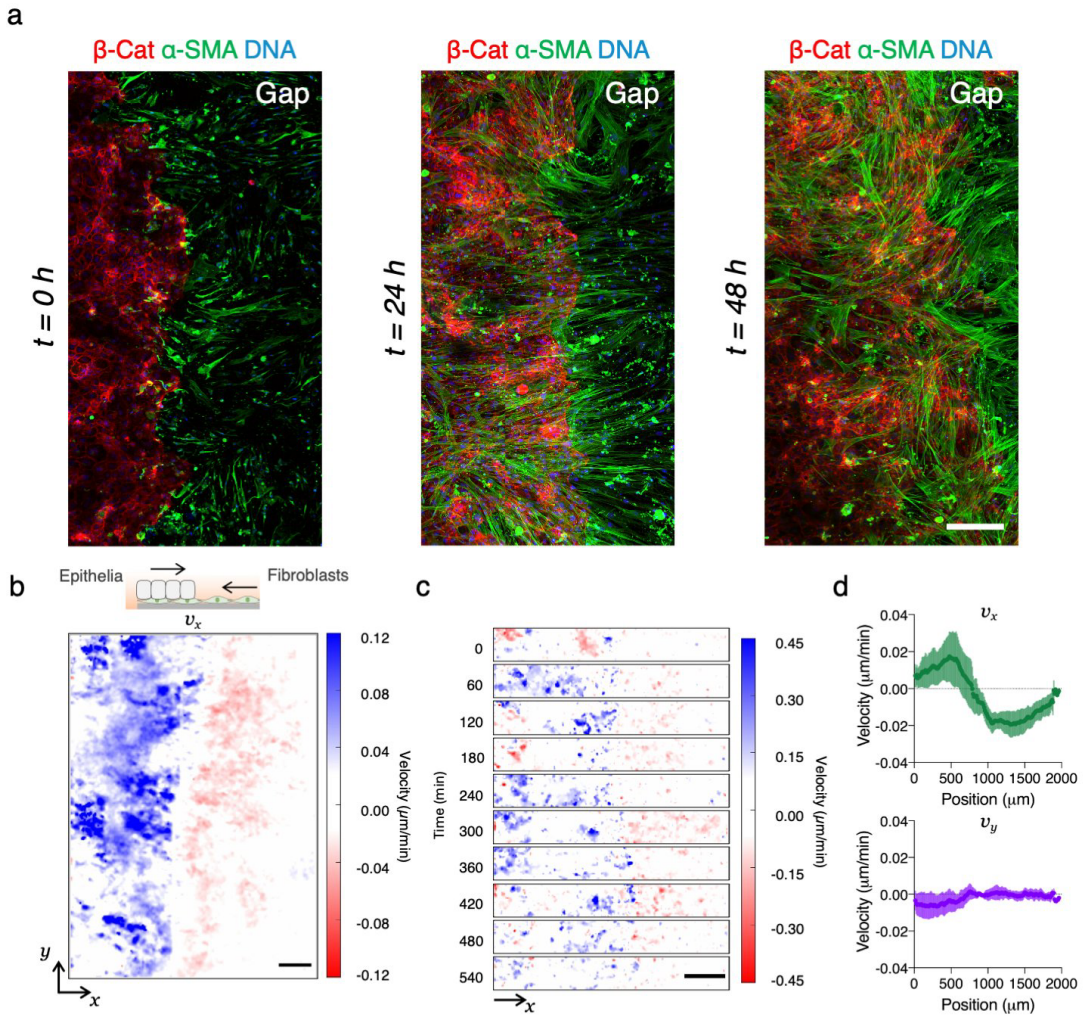

Figure 4. (a) Representative fluorescence microscopy images corresponding to immunostaining of β-Catenin (β-Cat), alpha-smooth muscle actin (α-SMA) and DNA of + fibroblasts condition. Timeframes corresponding to 0, 24 and 48h upon barrier removal. Scale bar: 100 μm. (b) Mean velocity in the x- component (v_x) during the first 9 hours of gap closure. Scale bar: 250 μm. (c) Snapshots of the instantaneous velocity v_x of a selected region along the first 9 hours of gap closure. Scale bar: 250 μm. (d) Profiles of the x-component (v_x) and y-component (v_y) of the mean velocity across the gap direction during the first 9 hours of gap closure. Mean ± SD of n = 4 migration fronts of N = 2 independent experiments.

The long-range organization of primary fibroblasts drives their coalignment with epithelial cells during gap closure

The above-mentioned observations suggest a coordinated and interactive migration process within the gap involving both IECs and the intestinal fibroblasts. So, to gain a deeper understanding of fibroblast movements during epithelial migration we decided to follow the dynamics of this process, we followed the dynamics of fibroblast rearrangement during epithelial migration (Figure 5a). Using primary fibroblasts expressing GFP at the cell membrane,[35] we examined their arrangement relative to the migration front and analyzed their orientation in the central region of the gap (Figure 5b). At the beginning of the experiment, we observed small swirly patterns in the orientation fields (Figure 5b), indicative of short-range alignments of polarity. However, over time, we observed a progressive alignment of fibroblasts perpendicular to the migration front (orientation vectors around 0º) (Figure 5b,c), resulting in the enlargement of the initial short-range alignments of polarity (Figure 5b). To visualize local discontinuities in alignment, we calculated the nematic order[36] for each vector grid. Over time, discontinuities between swirly patterns disappeared, indicating long-range alignments of polarity (Figure 5b), and the fraction of disordered regions (nematic order below 0.5)[37] decreased (Figure 5d). Notably, fibroblasts far away from the migration front (up to 750 μm) were also aligned, strongly suggesting a mechanism of fibroblast-fibroblast communication that results in a long-range order.

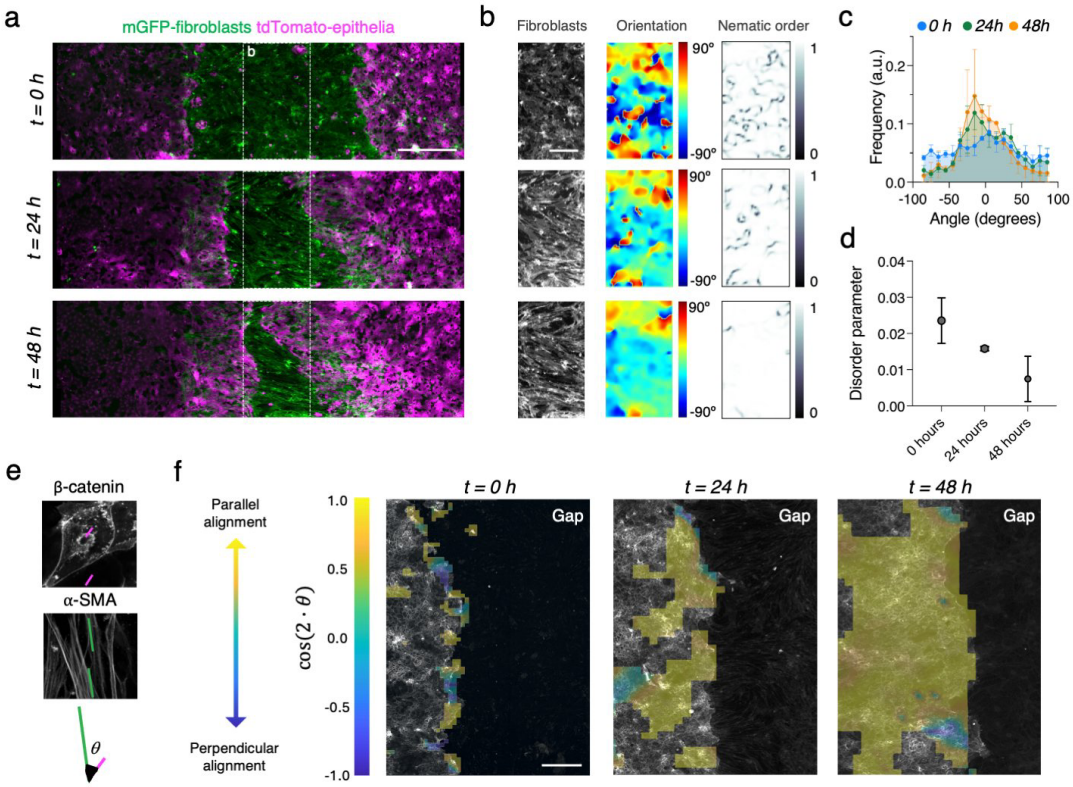

Figure 5. (a) Sum intensity projections of timeframes corresponding to 0, 24 and 48h upon barrier removal of the + fibroblasts condition. Scale bars: 500 μm. (b) Representative orientation and nematic order maps of fibroblasts in the central region of the gap (white box in a). Scale bar: 250 μm. (c) Angular distribution of fibroblast orientation at 0, 24 and 48h upon barrier removal. (d) Fibroblasts' disorder parameter over time. (e) Schematics depicting the dominant directions (ω) for each cell type and their angular difference θ, from which the correlation index ($\cos(2\cdot\theta)$) is defined. (f) Correlation maps at different time points (middle and right panels). Yellow stands for regions with parallel alignment between the two cell types and blue for regions with perpendicular alignment. Regions with no color indicate that at least one of the two cell types did not have a defined dominant direction. Scale bar: 500 μm. Immunostained samples from N = 2 independent experiments were used.

Next, we analyzed the temporal co-orientation of cells in the coculture during the gap closure by immunofluorescence using α-SMA and β-catenin antibodies to visualize fibroblasts and IECs, respectively. The dominant directions of fibroblasts and the IECs were computed by dividing the images in subregions (roughly of the area of an IEC) and determining their dominant directions (ω) from the spatial gradient of the fluorescent signal for β-catenin and for α-SMA (Figure 5e). We then calculated the angle (θ) between

the dominant directions of fibroblasts and IECs and plotted the value of cos(2·θ) (referred as correlation index, Figure 5f) for each subregion, generating correlation maps indicative of the alignment between the two cell types. The correlation analysis revealed that immediately after removing the barrier (t = 0 h), the alignment between fibroblasts and IECs was weak and restricted to the regions adjacent to the migration front (Figure 5f). However, as time went by (at 24 and 48 h), fibroblasts near the gap were more numerous, elongated (Figure 4a) and aligned with the IECs, becoming predominantly coaligned in the correlation map (Figure 5f, t = 24 and t = 48 h). This alignment extended further into the epithelium monolayer over time. Importantly, the accumulation of intestinal fibroblasts with high levels of α-SMA$^+$ stress fibers (Figure 4a) and the coalignment of fibroblasts and IECs matched temporally and spatially with the increased directionality of the epithelial trajectories towards closing the gap. This evidences the active role of fibroblasts, which appear to coordinate with IECs for an efficient epithelial migration.

Primary fibroblasts generate aligned ECM fibers to guide epithelial migration

In vivo, intestinal fibroblasts remodel the tissue matrix during wound healing through collagen deposition and metalloprotease expression.[9,38–42] Thus, we investigated whether this matrix deposition could contribute to the enhanced efficiency in epithelial gap closure observed in the physical presence of fibroblasts. Initially, we evaluated the matrix deposited by intestinal fibroblasts alone. A monolayer of fibroblasts was seeded and stained for α-SMA, vimentin, desmin, and for the ECM proteins fibronectin, laminin, and collagen IV. A significant portion of cells exhibited positive staining for α-SMA and vimentin (Figure S6a,b) while a few cells were positive for desmin (Figure S6c), confirming the presence of various subepithelial mesenchymal cell types.[14–16] These cells were found to express and secrete laminin (Figure S6a), fibronectin (Figure S6b), and collagen IV (Figure S6c). Subsequently, we investigated ECM protein deposition in the cocultures. Immunostaining of β-catenin, α-SMA, and collagen IV revealed organized collagen-path depositions accumulating between the fibroblast layer and the epithelium (Figure 6a,b), following the orientation patterns observed for the fibroblasts. This suggests that fibroblasts' secreted ECM facilitates epithelial migration.

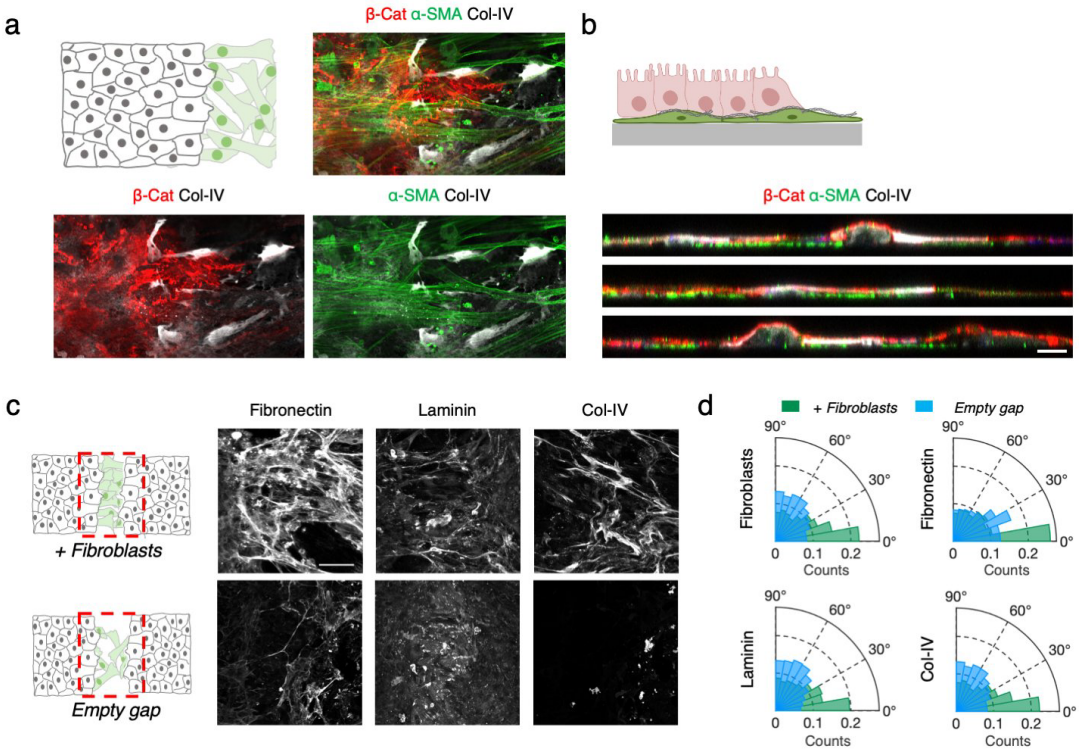

Figure 6. (a) Representative fluorescence microscopy images corresponding to immunostaining of β-Catenin (β-Cat), alpha-smooth muscle actin (α-SMA), and collagen-IV (Col-IV) in + fibroblasts condition. Scale bar: 25 μm. (b) Orthogonal cross-sections of the coculture. Scale bar: 10 μm. (c) Sum intensity projections of + fibroblasts and empty gap conditions at 24h upon barrier removal stained for fibronectin, laminin or col-IV. (d) Polar histograms of the fibbers' orientation of fibroblasts and each protein. 0º corresponds to parallel alignment to the migration direction and 90º, perpendicular.

To further explore this observation, we conducted immunostaining for fibronectin, laminin, and collagen IV near the migration front in the gaps of conditions with a continuous (+fibroblasts) and a discontinuous (empty gap) layer of fibroblasts. In gaps containing fibroblasts, a pronounced presence of fibronectin, laminin, and collagen IV was observed (Figure 6c), with these proteins organized in the form of fibers. In contrast, the amount of protein was dimmer and appeared more globular in the case of an empty gap (Figure 6c). We then checked the alignment of fibers and fibroblasts with the migration front and discovered that, for the fibroblast-free gap condition, the alignment was lost in fibroblasts near the migration front (Figure 6d). Moreover, when fibroblasts were in the gap, they aligned themselves together with fibronectin, laminin and collagen IV fibers parallel to the direction of epithelial migration. In the empty gap scenario, the

alignment was lost both for the ECM protein fibers and the fibroblasts near the migration front (Figure 6d). Altogether, these results suggest that the directional migration of epithelial cells is guided by the presence of aligned protein fibers secreted by the fibroblasts present in the gap region.

Primary intestinal fibroblasts lead to epithelial spreading in 3D cell cultures

Finally, we assessed the potential involvement of intestinal fibroblasts in epithelial spreading in a three-dimensional setting. We performed coculture experiments by embedding intestinal crypts and intestinal fibroblasts in 3D Matrigel drops (Figure 7a). Over a span of 4 days, we monitored the growth and morphological changes of the crypts in conditions analogous to those above: (i) crypts cultured with basic medium (control), (ii) crypts cultured with intestinal fibroblasts-derived conditioned medium (+ fibroblasts conditioned medium or + fibr. cond. med.), and (iii) crypts cocultured with intestinal fibroblasts in direct physical contact (+ fibroblasts). After 2 days in culture, control crypts developed into organoids with typical morphology consisting of bulging crypt-like regions and villus-like regions in between. However, in the presence of fibroblasts or their conditioned medium, organoids transformed into cystic structures lacking budding units (Figure 7b,c). The formation of cysts has been previously linked to an increase in proliferation.[16–18,43] Yet, we did not observe any increase in the proportion of Ki-67$^+$ cells in the conditioned medium samples compared to the control (Figure 7d). Instead, we found that while in the control condition, Ki-67$^+$ cells were localized in clusters within crypt-like regions, when cultured with conditioned medium, they were randomly distributed throughout the cysts. This cystic morphology of the organoids resembled that induced by BMP agonists[44] or by Prostaglandin E2 in the context of colonic wound healing.[27] Indeed, scRNAseq analysis revealed that the fibroblasts expressed factors involved in proliferation, such as Wnt2b and Rspo3, and differentiation, such as Bmp4 (Figure S1e). Thus, it appears that the paracrine signaling by the fibroblasts induces a morphological transition of organoids into cystic structures, which cannot be solely attributed to an increase in cell proliferation.

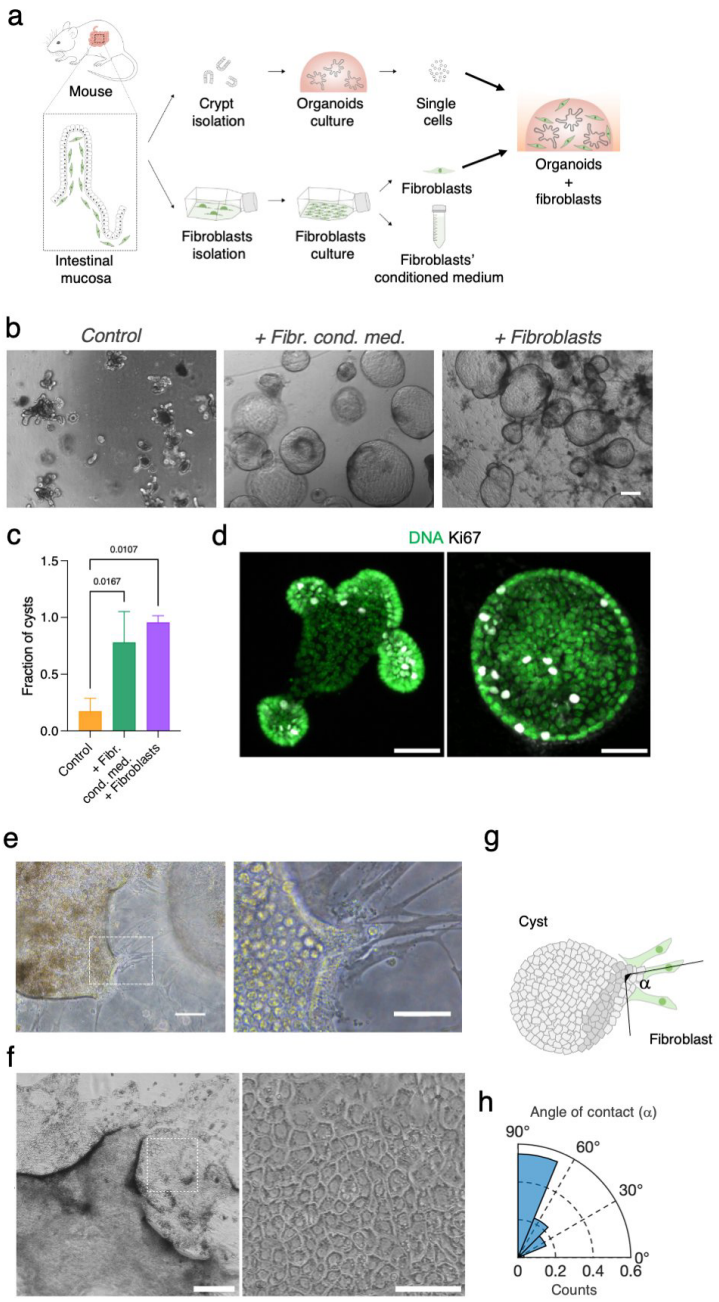

Figure 7. (a) Schematics of the experimental set-up. (b) Representative bright field images of crypts grown in 3D Matrigel® drops with ENRCV medium (*control*), with fibroblasts conditioned medium (+ *fibr. cond. med.*) and in coculture with primary fibroblasts (+ *fibroblasts*) after 2 days in culture. Scale bar: 1000 µm. (c) Fraction of cystic organoids respect to all organoids per condition. Mean ± SD. Kruskal-Wallis test. (d) Representative confocal images of crypts grown in 3D Matrigel® drops in *control* and in + *Fibr. cond. med.* Scale bars: 50 µm. (e) Phase contrast image of the expansion of epithelial cysts mediated by fibroblasts. Scale bar = 100 µm. Zoom-in scale bar = 50 µm. (f) Representative

bright field microscopy images of + fibroblasts condition after 14 days in culture. Scale bar: 250 μm. Zoom-in. Scale bar: 50 μm. (g) Schematics of the angle of contact between cysts and fibroblasts. (h) Distribution of the angle of contact between cysts and fibroblasts.

Moreover, while conditioned medium led to spherical cysts (Figure 7b, middle panel), cysts obtained in coculture with fibroblasts exhibited prominent bulging regions (Figure 7b, right panel), specially where in contact with fibroblasts (Movie 8). By day 4 of coculture, these bulging regions contacted the surrounding substrate (Figure 7e). Notably, fibroblasts appeared to trigger the expansion of the epithelium over the surface, leading to the transformation of cysts into flat monolayers exhibiting the characteristic hexagonal packing pattern of epithelial cells by day 14 of coculture (Figure 7f). Such spreading was not observed in cysts obtained when crypts were cultured with fibroblasts' conditioned medium alone. Upon closer examination, we observed that fibroblasts were arranged perpendicular to the cysts and were physically interacting with them (Figures 7g,h), suggesting a potential pulling of the fibroblasts on the epithelial cells. Thus, the coculture of organoids with fibroblasts induced a reorganization of 3D budding organoids into cystic structures and facilitated an expansion from 3D cysts to 2D monolayers. This epithelial migration required the physical contact between the organoids and the fibroblasts.

Discussion

During development,[2,45] in wound healing,[3–9] and cancer progression,[46–48] fibroblasts engage in physical crosstalk with epithelial cells. However, the impact of the physical presence of intestinal fibroblasts on intestinal epithelial migration remains poorly understood. In the late 1960's, colonic fibroblasts were suggested to migrate along the walls of crypts *in vivo* at a speed equivalent to that of epithelial cells, indicating a possible synchronized migration.[49] More recent work has shown the indispensable role of paracrine signals from intestinal mesenchymal cells recruited at the wound site in ensuring proper epithelial restoration *in vivo*.[24–27] Here, we demonstrate that the physical interaction between fibroblasts and epithelial cells plays a crucial role in guiding directed and persistent migration of organoid-derived intestinal epithelia. As epithelial migration begins, fibroblasts located at the gap become activated and migrate towards the epithelial front. Subsequently, fibroblasts further away from the migration front align themselves in the

direction of epithelial migration, secreting aligned ECM fibers. This coordinated action results in enhanced persistence and directionality of epithelial migration, facilitating successful closure of the gap. *In vivo*, colonic mesenchymal stem cells also migrate to wounds, indicating these cells have the potential to migrate from the adjacent mucosa to the site of epithelial injury.[26] In this context, *in vivo* epithelial cells undergo differentiation into a specific phenotype (WAE cells), which is responsible for repopulating the damaged intestine and restoring tissue integrity. Notably, we observed a significant migration of fibroblasts from the gap region to the leading edge of the epithelia, coinciding in time with the onset of migration of the intestinal epithelial cells.

Interestingly, when studying the physical interaction between fibroblasts and epithelial cells in a 3D reconstituted basement membrane gel we observed that the recruitment of intestinal fibroblasts and their close interaction with epithelial cells were necessary for the opening of enclosed epithelial cysts and the subsequent formation of epithelial monolayers. This was clearly shown by the arrangement of fibroblasts perpendicular to the epithelial tongues leading epithelial spreading in 3D, as well as in 2D. This arrangement resembles certain observations in pathological conditions like cancer, where cancer associated fibroblasts (CAFs) engage in physical interactions with epithelial tumors, promoting their migration and aiding invasion.[50] Interestingly, this perpendicular arrangement was not restricted to the vicinity of the epithelial front. On the contrary, fibroblasts far from the epithelial front and at the center of the gap aligned and oriented themselves parallel to the migration direction of the epithelial cells. This phenomenon, known as long-range ordering or nematic ordering, has been described in the context of polar filaments,[51] the tumor microenvironment,[52] muscle differentiation,[37,53] bacterial colonies[54] and confined monolayers,[55–57] and it resulted to be key in the cells' ability to fully close the gap in our experiments. Epithelial cells coaligned with the underlaying fibroblasts, and the absence of a continuous monolayer of such cells led to a decrease in epithelial persistence and directionality.

Moreover, the enhanced efficiency in gap closure of our *in vitro* model was not related with an enhanced cell proliferation, which may solely act as a mechanism to replace dead cells.[24,58] Instead, we speculate that both proliferative and differentiation signals from intestinal fibroblasts might boost the dynamics of epithelial tissue turnover. Indeed, a fundamental aspect for effective gap closure is the preservation of epithelial integrity throughout the process.[59] The advancement of the tissue must occur while maintaining

cell-cell contacts. This is an active process involving cell proliferation, delamination of dead cells, changes in cell shape and tissue rearrangements.[60] Interestingly, we observed the emergence of holes within the monolayer during migration in our experiments. This resulted in complete loss of tissue integrity in the control condition, and partial loss in the presence of fibroblasts' conditioned medium. On the contrary, when fibroblasts were physically present, the gaps that emerged during epithelial migration promptly closed. In a recent study using MDCK monolayers,[61] the appearance of holes was linked to events such as cell division or cell stretching, which aligns with our observations, as gaps often appeared adjacent to large cells. This phenomenon is attributed to a monolayer experiencing tensile stress,[61] which is indeed dominant within a migrating epithelium such as ours.[62]

Conclusions

In summary, our study has demonstrated the active involvement of primary intestinal fibroblasts in orchestrating epithelial migration *in vitro*, encompassing both 2D and 3D settings. Their presence, accompanied by their self-organization stablishing long-range order and the secretion of aligned extracellular matrix fibers, significantly contributes to the enhancement of gap closure and the upholding of epithelial integrity. Our findings showed that intestinal fibroblasts, situated at a distance from the migrating epithelium activated and migrated towards the epithelial front, where they aligned to the direction of the advancing epithelium. In parallel, in the central region of the gap, they were able to self-organize and align themselves in accordance with the advancing direction of the epithelial cells. Concurrently, these fibroblasts secreted aligned extracellular matrix protein fibers, which functioned as guiding tracks, facilitating the onward movement of epithelial cells and fostering more persistent and directed migration resulting in a more efficient gap closure. Considering the intestinal epithelium's crucial function as a protective physical barrier that prevents external insults to come into contact with the immune system of the lamina propria, the rapid and effective repair of epithelial damage is of paramount importance in maintaining intestinal equilibrium and averting uncontrolled inflammatory reactions.[63,64] In this context, we propose a novel function for intestinal fibroblasts, serving as pivotal agents in the restoration of intestinal epithelium by regulating both epithelial migration and integrity.

Materials and Methods

Mouse models

All experimental protocols involving mice were approved by the Animal care and Use Committee of Barcelona Science Park (CEEA-PCB) and the Catalan government and performed in accordance with their relevant guidelines and regulations. *Lgr5-EGFP-IRES-creERT2* mice have been previously described.[65] Briefly, *Lgr5-EGFP-IRES-creERT2* mice were generated by homologous recombination in embryonic stem cells targeting the *EGFP-IRES-creERT2* cassette to the ATG codon of the stem cell marker *Lgr5* locus, allowing the visualization of $Lgr5^+$ stem cells with a green fluorescent protein (GFP). *Lgr5-EGFP-IRES-creERT2* mice were crossed with the Cre reporter strain Ai9 (RCL-tdT) (JAX-007909) to generate the *Lgr5-EGFP-IRES-creERT2/RCL-tdT mouse*. Ai9 (RCL-tdT) is designed to have a *loxP*-flanked STOP cassette preventing transcription of the CAG promoter-driven red fluorescent variant (tdTomato), inserted into the *Gt(ROSA)26Sor* locus. Upon Cre-mediated recombination *Lgr5-EGFP-IRES-creERT2/RCL-tdT* mice express robust tdTomato fluorescence in Lgr5-expressing cells and their progeny. *ROSA26-creERT2;mT/mG* (henceforth mTmG) mouse model consists of a cell membrane-targeted, two-color fluorescent Cre-reporter allele. Prior to Cre recombination, cell membrane-localized tdTomato (mT) is expressed in all tissues. Upon the activation of Cre recombinase through tamoxifen, all cells (and future cell lineages derived from these cells) express cell membrane localized GFP (mG) instead of mT.

Intestinal crypts isolation and culture

Intestinal crypts from *Lgr5-EGFP-IRES-creERT2/RCL-tdT* mice were isolated as previously described.[35,66] Briefly, small intestines were flushed with PBS and cut longitudinally. Villi were mechanically removed, and intestinal crypts were isolated by incubating the tissue with PBS containing 2 mM EDTA (Sigma) for 30 minutes at 4°C. The digestion content was filtered through a 70 µm pore cell strainer (Biologix Research Co.) to obtain the crypt fraction. Crypts were plated in Matrigel® (BD Bioscience) drops and supplemented with basic medium: advanced DMEM/F12 (Invitrogen) plus 1% Glutamax (Gibco), 1% HEPES (Sigma), Normocin (1:500, Invitrogen), 2% B27 (Gibco), 1% N2 (Gibco), 1.25 mM N-acetylcysteine (Sigma), supplemented with recombinant murine EGF (100 ng mL^{-1}, Gibco), recombinant human R-spondin 1 (200 ng mL^{-1}, R&D Biosystems), and recombinant murine Noggin (100 ng mL^{-1}, Peprotech), CHIR99021 (3 µM, Tebu-bio) and valproic acid (1 mM, sigma) to formulate the ENRCV medium.[67] The medium was

changed every 2 to 3 days. The first 4 days of culture the Rho kinase inhibitor Y-27632 (Sigma) was added to the culture. Outgrowing crypts were passaged once a week and organoid stocks were maintained for up to 4 months.

Generating Lgr5-EGFP/RCL-tdT intestinal organoids by in vitro tamoxifen dependent creERT2 induction

Lgr5-EGFP-IRES-creERT2/RCL-tdT small intestinal organoids were treated *in vitro* with 100 nM of 4-Hydroxitamoxifen (4-HT) (Sigma) for 48 h to induce the expression of tdTomato in Lgr5$^+$ cells. Treated intestinal organoids were mechanically and enzymatically digested as described above and cell sorted to obtain pure GFP$^+$ and tdTomato$^+$ cell populations. Sorted cells were cultured in Matrigel® drops with ENRCV medium plus the Rho Kinase inhibitor Y-27632 (Sigma) to obtain a new *in vitro* line of intestinal organoids named *Lgr5-EGFP/RCL-tdT,* which expresses a robust tdTomato fluorescence in all cells and GFP fluorescence in Lgr5$^+$ stem cells. Outgrowing crypts were passaged once a week and organoid stocks were maintained for up to 4 months.

Intestinal organoid digestion to single cells

To obtain organoid-derived intestinal epithelial cells (IECs), organoids were first obtained from *Lgr5-EGFP-IRES-creERT2/RCL-tdT* mice. Then, fully-grown organoids were subjected to a digestion protocol. Briefly, Matrigel® drops containing organoids were disrupted by pipetting with TrypLE Express1X (Gibco) and transferred to a Falcon tube at 4°C, where mechanical disruption was applied using a syringe with a 23 G 1” needle (BD Microlance 3). Disrupted organoids were further digested by incubating them for 5 to 7 minutes at 37ºC with vigorous hand-shaking every minute. Successful digestion to single cells was confirmed via inspection under the microscope.

Intestinal fibroblasts’ isolation and culture

Intestinal primary fibroblasts were isolated from the same three models used to establish organoids’ culture. Lgr5-GFP- and tdTomato-derived stromal cells exhibited a wild-type phenotype (no fluorescence). mTmG-derived stromal cells exhibited cell membrane-localized tdTomato fluorescence (mT). Intestinal primary fibroblasts were isolated from mouse small intestine by adapting a previously published protocol.[68] Briefly, once the crypts were isolated, the tissue pieces were further digested by first performing 3 incubations of 10 min with 3 mM EDTA in PBS containing at 37ºC shaking. Next, after a washing with PBS, the pieces

were incubated with collagenase (100 U mL^{-1}) (Sigma-Aldrich) in culture medium for 30 minutes at 37ºC shaking. Then, the tissue was centrifuged at 1200 rpm for 5 min and the pellet was resuspended in DMEM (1X) with GlutaMAX™ (Gibco) medium supplemented with 10% FBS, 1% Penicillin-Streptomycin (Sigma-Aldrich) and 1% v/v minimum essential medium non-essential amino acids (MEM-NEAA; Gibco) (primary fibroblasts culture medium). The tissue pieces were cultured in flasks kept at 37°C in a humidified incubator under a 5% CO_2 atmosphere. After seven days in culture, tissue pieces had attached, and fibroblasts started to come out and attach to the flasks. Plates reached confluency after approximately fourteen days. Primary fibroblasts were passaged with a split ratio of 1:2 or 1:3, by first rinsing the cells with warm PBS and incubating them with Trypsin-EDTA (Life Technologies) for 5 minutes at 37°C. Next, Trypsin-EDTA was neutralized by adding an equal volume of culture medium and cells were centrifuged at 1200 rpm for 5 min. The supernatant was discarded, the pellet was resuspended in culture medium, and the proportional volume was seeded in a new flask containing warm culture medium. Primary fibroblasts were only passaged a maximum of 5 times. mTmG-derived fibroblasts were treated with 4-HT (Merck Life Science) for seven days to convert them from mT+ to mG+ fibroblasts.

Preparation of primary fibroblasts conditioned medium

The culture medium used to grow the primary fibroblasts for 4-6 days was collected, centrifuged, and filtered through a 0.22 µm pore size filter (Merck-Millipore). Next, it was supplemented with 2% B27, 1% N2 and 0.25% N-acetylcysteine, obtaining primary fibroblast_CM. To render it suitable for the culture of organoids or organoid-derived cells, the primary fibroblast_CM was supplemented with EGF (100 ng mL^{-1}), human R-Spondin 1 (200 ng mL^{-1}), Noggin (100 ng mL^{-1}), CHIR99021 (3 mM), valproic acid (1 mM), resulting in primary fibroblast_CM/ENRCV.

Single cell RNA sequencing of primary fibroblasts

To characterize the different cell populations within the isolated stromal cells, we performed single cell RNA sequencing (scRNAseq). A pool of 3 vials of primary fibroblasts from 3 different isolations at passage 2-4 was prepared to remove the possible variability coming from the mouse selected. Briefly, the 3 vials were centrifuged at 335 rcf during 5 min at 4ºC and resuspended in DMEM/F12 with 10% FBS so as to have a cell density of 300-1000 cells μL^{-1}. Cell concentration and viability were determined using a TC20™ Automated Cell Counter (Bio-Rad Laboratories, S.A) upon staining the cells with Trypan blue. Cells were

partitioned into Gel Bead-In-Emulsions (GEMs) by using the Chromium Controller system (10X Genomics), with a target recovery of 5000 total cells. cDNA sequencing libraries were prepared using the Next GEM Single Cell 3' Reagent Kits v3.1 (10X Genomics, PN-1000268), following manufacturer's instructions. Shortly, after GEM-RT clean up, cDNA was amplified during 12 cycles and cDNA quality control and quantification were performed on an Agilent Bioanalyzer High Sensitivity chip (Agilent Technologies). cDNA libraries were indexed by PCR using the PN-220103 Chromiumi7 Sample Index Plate. Size distribution and concentration of 3' cDNA libraries were verified on an Agilent Bioanalyzer High Sensitivity chip (Agilent Technologies). Finally, sequencing of cDNA libraries was carried out on an Illumina NovaSeq 6000 using the following sequencing conditions: 28 bp (Read 1) + 8 bp (i7 index) + 0 bp (i5 index) + 89 bp (Read 2), to obtain approximately 20-30.000 reads per cell.

Sequencing reads were processed using CellRanger v.6.1.2 (Zheng et al., 2017). The output folder was used as input to perform downstream analysis with the R package Seurat 4.0.6 (R.4.1.2). Seurat object was created with the function CreateSeuratObject with the parameter min.cells = 3. To ensure cells of good quality, only cell barcodes within the range of 2000 - 7000 detected genes and < 5 % mitochondrial content were kept for the analysis. Data was normalized with the SCTransform method with default parameters. UMAP was performed with the 30 first principal components, followed by the functions FindNeighbours and FindClusters with default resolution. Cluster markers were identified with the function FindAllMarkers with the options only.pos = TRUE and logfc.threshold = 0.25 . Cell type annotation was performed manually looking the expression of the following cell type markers: telocytes = c("Wnt4", "Wnt5a", "Wnt5b", "Dkk3", "Wif1", "Chrd", "Bmp1", "Bmp2", "Bmp4", "Bmp5", "Bmp7", "Acta2", "Vim", "Pdgfra", "Foxl1", "Myh11", "Gli1", "Cspg4", "Pdpn"); trophocytes = c("Wnt2b", "Rspo1", "Rspo2", "Rspo3", "Dkk2", "Dkk3", "Srfp1", "Grem1", "Bmp4", "Vim", "Pdgfra", "Cd34", "Gli1", "Cd81"); PDGFRlow_stroma = c("Wnt2b", "Wnt4", "Rspo3", "Dkk2", "Dkk3", "Srfp1", "Frzb", "Grem1", "Bmp1", "Bmp2", "Bmp4", "Bmp5", "Bmp6", "Vim", "Pdgfra", "Cd34", "Gli1", "Cspg4", "Pdpn"); pericytes = c("Grem2", "Acta2", "Vim", "Des", "Myh11", "Cspg4", "Actg2", "Pdgfrb", "Rgs5"); neurons = c("Wnt6", "Gfap", "S100b"); immune cells = c("Bmp1", "Cd52"); lymphatic cells = c("Lyve1"); blood cells = c("Pecam1").

Coculture of intestinal organoids with primary fibroblasts

To test the effect of culturing primary fibroblasts with intestinal organoids, crypts derived from Lgr5-EGFP-IRES-creERT2 intestinal organoids were embedded in Matrigel drops together with primary fibroblasts and cultured with ENRCV medium. To test only the paracrine effect of primary fibroblasts, crypts were cultured alone with primary fibroblast_CM/ENRCV medium. Crypts were also cultured alone using ENRCV medium. Cultures were maintained for 2 days.

Setup of the gap closure models

Ibidi μ-Slides 8 wells (Ibidi GmbH) were coated with Matrigel® to form thin films (< 2 μm) as an extracellular matrix (ECM) surrogate as previously described.[30,32] Briefly, Ibidi wells were coated with 10 μL cm^{-2} of 3 mg mL^{-1} Matrigel® diluted in DMEM/F-12 (Invitrogen). To spatially confine cell growth and create a gap where cells could migrate to, we employed PDMS barriers fabricated in-house. For the "control" condition, first the elastomeric barrier was placed and stuck (using PDMS grease, Corning) on the Matrigel® coated wells. Then, $3.5x10^5$ organoid-derived cells cm^{-2} were seeded with ENRCV medium containing Y-27632 and cells were cultured for 1 day. For the "+ fibr. cond. med." condition, the elastomeric barrier was placed as in the control condition, then organoid-derived cells were seeded with primary fibroblast_CM/ENRCV medium containing Y-27632, and cells were cultured for 1 day. For the "+ fibroblasts" condition, first, $3x10^4$ primary fibroblasts cm^{-2} were seeded on the Matrigel® coated well and cultured with primary fibroblasts culture medium for 1 day, then the elastomeric barrier was placed, and $3.5x10^5$ organoid-derived cells cm^{-2} were seeded on top with ENRCV medium containing Y-27632 for 1 day more. Finally, for the "empty gap" condition, first the elastomeric barrier was placed and stuck (using PDMS grease, Corning) on the Matrigel® coated wells. Then, $3x10^4$ primary fibroblasts cm^{-2} were seeded on the Matrigel® coated well and cultured with primary fibroblasts culture medium for 1 day, then $3.5x10^5$ organoid-derived cells cm^{-2} were seeded on top with ENRCV medium containing Y-27632 for 1 day more. After the indicated times, the migration assay was initiated by carefully removing the elastomeric barrier, washing with warm PBS and adding new corresponding medium without Y-27632.

Immunostaining and image acquisition of fixed samples

Cells in Ibidi μ-Slides wells were fixed with 10% neutralized formalin, permeabilized with 0.5% Triton X-100 for 30 minutes, and blocked with 1% BSA, 3% donkey serum, and 0.2% Triton X-100 in PBS for 2 h at RT. Samples were then incubated with the primary antibodies against Ki-67, fibronectin, laminin and collagen I

(Table 1) overnight at 4°C followed by several PBS washings. Next, samples were incubated with the adequate secondary antibodies (Table 2) plus DAPI (1:1000, Thermo Fisher Scientific) and rhodamine-phalloidin (3.5:500, Cytoskeleton) for 2 h at RT. Finally, samples were washed with PBS and mounted with Fluoromount G (Southern Biotech). Fluorescence images were acquired using a confocal laser scanning microscope (LSM 800, Zeiss) with a 10x objective (NA = 0.3, WD = 2.0) or 20x objective (NA=0.8, WD=0.55). The laser excitation and emission light spectral collection were optimized for each fluorophore. The pinhole diameter was set to 1 Airy Unit (AU).

Live imaging

To optimally track the epithelial cells, single cells derived from tdTomato organoids treated with *4-HT* (all cells tdTomato+) and from Lgr5-GFP organoids (only stem cells GFP+) were mixed in a 2:1 ratio, respectively, to reduce the number of fluorescent cells and thus ease cell detection and therefore tracking. Similarly, primary fibroblasts isolated from mTmG mice and treated with *4-HT* (mG+) were used in the time-lapse experiments. To register the migration, an Axio Observer 7 epifluorescence inverted microscope (Zeiss) with a 10x objective or a LEICA Thunder with 10x objective (NA=0.32, WD= 11.13) or 20x objective (NA=0.4, WD=7.5-6.2), employing temperature (37°C), relative humidity (95%), and CO_2 (5%) control were used. Phase contrast, Alexa 546 and Alexa 488 channels were employed. Images were acquired every 10 min up to 48 h of culture.

Fraction of cysts and angle of contact

The fraction of cysts respect to total number of organoids (cysts and budding organoids) was calculated by manual counting of control n = 186 organoids of N = 7 independent experiments, + fibr. cond. med. n = 151 organoids of N = 6 experiments, and + fibroblasts n = 167 organoids of N = 4 experiments. The angle of contact was measured as the angles between the fibroblast's long axis and the tangent to the cyst. Measurements were obtained from n = 30 fibroblasts from N = 2 experiments.

Frequency of Ki-67$^+$ epithelial cells

Confocal fluorescence microscopy images of Ki-67 marker were used to quantify the proliferative cells at t=24h. In Imaris, nuclei were first detected with the Imaris Spot detector (diameter set to 9 µm) by manually adjusting the threshold. Next, we applied a F-Actin mean intensity filter to only analyse nuclei within the epithelial monolayer. Then, positive cells for Ki-67 were filtered by applying a threshold of the mean intensity

of the marker. Finally, the percentage of Ki-67$^+$ cells respect to the total number of cells was computed. N = 3 independent experiments for control, N = 2 for + fibr. cond. med. and N = 2 for + fibroblasts were analyzed.

Fraction of gap closed

In Fiji *(http://rsb.info.nih.gov/ij, NIH, USA)*, the cell-free area was measured for frames of cell migration videos every hour and they were normalized to the final cell-free area to obtain the fraction of gap closed. N = 4 independent experiments for control, N = 2 for + fibr. cond. med., N = 3 for + fibroblasts, and N = 4 for empty gap, were analyzed.

Analysis of holes

Holes appearing in the epithelia during gap closure were analyzed by manually outlining the area of each hole in every time point. Hole area was normalized by the maximum area achieved by each hole during its lifetime. $n_{control}$ = 4 holes, $n_{fib.\ cond.\ med.}$ = 10 holes, and n_{+fib} = 4 holes, from N ≥ 2 independent experiments were analyzed.

Cell migration analysis

The centroid trajectories of *Lgr5-EGFP/RCL-tdT* cells were tracked using the Manual Tracking Plug-in in Fiji. Data analysis was performed using a custom-made code in Matlab (Mathworks, USA). Cell centroid positions during the experiment were defined as $\mathbf{r}_i = \mathbf{r}(i\Delta t)$, being Δt the time between consecutive images and **r** a vector. The vector difference between the initial ($t = t_0$) and the final point ($t = t_f$) is defined as the displacement vector **d** and its module $\| \mathbf{d} \|$ as the net displacement. The alignment index of the trajectories is defined as $\cos(2\cdot\alpha)$, being α the angle between the displacement vector **d** and the gap direction, defined as the direction perpendicular to the epithelial edge. This index equals 1 when the trajectory is parallel to the direction of the gap and -1 when it is perpendicular. For the cell migration analysis, $n_{control}$ = 132 cells, $n_{fib.\ cond.\ med.}$ = 138 cells, n_{+fib} = 205 cells, and n_{empty} = 118 cells randomly distributed within the epithelia from N ≥ 3 independent experiments were analyzed. PIVlab 2.37[69] was used to quantify the displacements of IECs and intestinal fibroblasts on phase contrast time-lapse movies. Briefly, an interrogation window of 23 µm with a step of 11.5 µm was used to perform Particle Image Velocimetry (PIV) either by FFT window deformation or by ensemble correlation. Image sequencing was set as time-resolved and the resulting velocities were filtered using a standard deviation filter (8*STD) and a local median filter (threshold = 3). For the PIV analysis, n = 4 migration fronts from N = 2 independent experiments were used.

Cell orientation analysis

Orientation fields were obtained using the OrientationJ[70] plug-in in Fiji. For fibroblasts orientation and nematic order, the ROIs were analyzed using a structure tensor local window of 20 pix and a grid size of 20 pix. Nematic order was measured as $S(x,y) = \sqrt{\langle \cos(2\theta) \rangle_{(x,y)}^2 + \langle \sin(2\theta) \rangle_{(x,y)}^2}$, where q is the local orientation of fibroblasts obtained from OrientationJ. Brackets < > denote an average over a local region of interest (x,y) which was defined by 4x4 grid positions each. The fraction of disorder parameter is calculated as the fraction of local regions of interest for which the local nematic order parameter S is below a threshold of 0.5. Images from N = 3 independent experiments were used. For the correlation of cell orientations between fibroblasts and IECs, we proceeded as follows. First, images were pre-processed by subtracting the background (40 pixels rolling ball), then a band-pass filter was applied (limits 3 and 40 pixels), and the background noise was subtracted again (40 pixels rolling ball). The resulting images were processed with OrientationJ using a local window of 40 pixels to obtain a structure tensor on a grid of 40 pixels x 40 pixels. With vector fields and their associated values provided by the plug-in (dominant direction ω, energy E and coherence C) we used a custom-made Matlab code to determine the correlation maps. Briefly, we selected the angles with associated energy E > 0.1 and coherency C > 0.05 for each cell type (IEC or intestinal fibroblasts) and discarded the rest. These sets of angles were used to calculate the mean cell orientation and the correlation index. To do so, we collected pairs of dominant angles and obtained the difference between them $\theta = \omega_{IEC} - \omega_{intestinal\ fibroblasts}$ for each x, y position within the image (note that we only accounted for x, y positions when the dominant angles for both cell types satisfied the conditions for E and C). Then, we defined the correlation index between the two cell types as $\cos(2\cdot\theta)$, which equals 1 when both cells are oriented parallel to each other and -1 when they are perpendicularly oriented. For this analysis, we used immunostained samples from N = 2 independent experiments.

Orientation of fibroblasts and deposited proteins

For + fibroblasts and empty gap conditions, orientation fields of fibroblasts at t = 0, 24 and 48 h after barrier removal and of deposited proteins at t=24h were obtained using the OrientationJ plug-in in Fiji using a local window of 2 pixels. Next, the fraction of vector fields respect to the total was computed for each bin spanning 10 degrees. Then, polar histograms were generated in Matlab. For orientation analysis of fibroblasts, we

analyzed 14 pictures from N = 5 independent experiments. For orientation analysis of deposited proteins, we analyzed: laminin = 4 ROIs from N = 1, fibronectin = 4 ROIs from N = 2, and collagen IV = 6 ROIs from N = 3.

Statistics

No statistical methods were used to predetermine sample size. Measurements were performed on experimental replicates (n) obtained in different independent experiments (N). Data presentation (as Mean value ± standard deviation (SD) or as Mean value ± standard error of the mean (SE)) is defined at the corresponding figure caption. D'Agostino normality test, t-test, and Kruskal-Wallis test were performed using GraphPad Prism 9. Specific values are noted at the corresponding figure captions.

Acknowledgements

We thank the Martinez Lab members and R.Sunyer for discussions and help, and O. Castillo for assistance in preparing the PDMS barriers.

The authors wish to acknowledge the MicroFabSpace and Microscopy Characterisation Facility, Unit 7 of ICTS "NANBIOSIS" from the CIBER-BBN at IBEC.

Funding for this project was provided by:

European Union Horizon 2020 ERC grant (agreement no. 647863 - COMIET).

Department of Research and Universities of the Generalitat de Catalunya (2021 SGR 01495).

CERCA Programme/Generalitat de Catalunya.

Networking Biomedical Research Center (CIBER) of Spain. CIBER is an initiative funded by the VI National R&D&i Plan 2008-2011, Iniciativa Ingenio 2010, Consolider Program, CIBER Actions and the Instituto de Salud Carlos III (RD16/0006/0012), with the support of the European Regional Development Fund (ERDF).

Grant PID2021-129115OB-I00 funded by MCIN/AEI/ 10.13039/501100011033 and by "ERDF A way of making Europe".

The results presented here only reflect the views of the authors; the European Commission is not responsible for any use that may be made of the information it contains.

References

1. Sherwood, D. R. Basement membrane remodeling guides cell migration and cell morphogenesis during development. *Current Opinion in Cell Biology* vol. 72 19–27 Preprint at https://doi.org/10.1016/j.ceb.2021.04.003 (2021).
2. Ewald, A. J., Brenot, A., Duong, M., Chan, B. S. & Werb, Z. Collective Epithelial Migration and Cell Rearrangements Drive Mammary Branching Morphogenesis. *Dev Cell* **14**, 570–581 (2008).
3. Davies, D. E. The Bronchial Epithelium in Chronic and Severe Asthma. *Curr Allergy Asthma Rep* **1**, 127–133 (2001).
4. Gabbiani, G., Ryan, G. B. & Majno, G. Presence of modified fibroblasts in granulation tissue and their possible role in wound contraction. *New York* 549–550 (1971).
5. Gorono, R. M. R. *et al.* Radial Keratofomy //. Role of rhe Myofibroblosr in Corneol Wound Conrrocrion. **33**, 3271–3282 (1992).
6. Jester, J. V., Petroll, W. M. & Cavanagh, H. D. Corneal stromal wound healing in refractive surgery: The role of myofibroblasts. *Prog Retin Eye Res* **18**, 311–356 (1999).
7. Chitturi, R. T. *et al.* The role of myofibroblasts in wound healing, contraction and its clinical implications in cleft palate repair. *J Int Oral Health* **7**, 75–80 (2015).
8. Hinz, B. The myofibroblast: Paradigm for a mechanically active cell. *J Biomech* **43**, 146–155 (2010).
9. Tomasek, J. J., Gabbiani, G., Hinz, B., Chaponnier, C. & Brown, R. A. Myofibroblasts and mechano: Regulation of connective tissue remodelling. *Nat Rev Mol Cell Biol* **3**, 349–363 (2002).
10. Powell, D. W., Adegboyega, P. A., Di Mari, J. F. & Mifflin, R. C. Epithelial cells and their neighbors: I. Role of intestinal myofibroblasts in development, repair, and cancer. *Am J Physiol Gastrointest Liver Physiol* **289**, 2–7 (2005).
11. Federici, T. & Boulis, N. M. Myofibroblasts II Intestinal subepithelial myofibroblasts. *Invited Review* A (1999) doi:10.1227/01.neu.0000335653.52938.f2.
12. Richman, P. I., Tilly, R., Jass, J. R. & Bodmer, W. F. Colonic pericrypt sheath cells: characterisation of cell type with new monoclonal antibody. *J Clin Pathol* **40**, 593 (1987).
13. Mifflin, R. C., Pinchuk, I. V, Saada, J. I. & Powell, D. W. Intestinal myofibroblasts: targets for stem cell therapy. *American Journal of Physiology-Gastrointestinal and Liver Physiology* **300**, G684–G696 (2011).
14. McCarthy, N., Kraiczy, J. & Shivdasani, R. A. Cellular and molecular architecture of the intestinal stem cell niche. *Nat Cell Biol* **22**, 1033–1041 (2020).
15. Lahar, N. *et al.* Intestinal subepithelial myofibroblasts support in vitro and in vivo growth of human small intestinal epithelium. *PLoS One* **6**, 1–9 (2011).
16. Lei, N. Y. *et al.* Intestinal subepithelial myofibroblasts support the growth of intestinal epithelial stem cells. *PLoS One* **9**, (2014).
17. Farin, H. F., Van Es, J. H. & Clevers, H. Redundant sources of Wnt regulate intestinal stem cells and promote formation of paneth cells. *Gastroenterology* **143**, 1518-1529.e7 (2012).
18. Kabiri, Z. *et al.* Stroma provides an intestinal stem cell niche in the absence of epithelial Wnts. *Development (Cambridge)* **141**, 2206–2215 (2014).
19. He, X. C. *et al.* BMP signaling inhibits intestinal stem cell self-renewal through suppression of Wnt–β-catenin signaling. *Nat Genet* **36**, 1117–1121 (2004).
20. Kosinski, C. *et al. Gene Expression Patterns of Human Colon Tops and Basal Crypts and BMP Antagonists as Intestinal Stem Cell Niche Factors*. www.pnas.org/cgi/content/full/ (2007).
21. McCarthy, N. *et al.* Distinct Mesenchymal Cell Populations Generate the Essential Intestinal BMP Signaling Gradient. *Cell Stem Cell* **26**, 391-402.e5 (2020).
22. Jardé, T., Kerr, G., Akhtar, R. & Abud, H. E. Modelling intestinal carcinogenesis using in vitro organoid cultures. *Methods in Molecular Biology* **1725**, 41–52 (2018).
23. Huycke, T. R. *et al.* Patterning and folding of intestinal villi by active mesenchymal dewetting. *bioRxiv* (2023) doi:10.1101/2023.06.25.546328.
24. Seno, H. *et al.* Efficient colonic mucosal wound repair requires Trem2 signaling. *Proc Natl Acad Sci U S A* **106**, 256–261 (2009).

25. Hiroyuki Miyoshi, Rieko Ajima, Christine T. Luo, Terry P. Yamaguchi & Thaddeus S. Stappenbeck. Wnt5a Potentiates TGF-b Signaling to Promote Colonic Crypt Regeneration After Tissue Injury. *Science (1979)* **338**, 108–113 (2012).
26. Manieri, N. A., Drylewicz, M. R., Miyoshi, H. & Stappenbeck, T. S. Igf2bp1 is required for full induction of Ptgs2 mRNA in colonic mesenchymal stem cells in mice. *Gastroenterology* **143**, (2012).
27. Miyoshi, H. *et al.* Prostaglandin E2 promotes intestinal repair through an adaptive cellular response of the epithelium. *EMBO J* **36**, 5–24 (2017).
28. Seltana, A., Basora, N. & Beaulieu, J. F. Intestinal epithelial wound healing assay in an epithelial-mesenchymal co-culture system. *Wound Repair and Regeneration* **18**, 114–122 (2010).
29. Thorne, C. A. *et al.* Enteroid Monolayers Reveal an Autonomous WNT and BMP Circuit Controlling Intestinal Epithelial Growth and Organization. *Dev Cell* **44**, 624-633.e4 (2018).
30. Altay, G. *et al.* Self-organized intestinal epithelial monolayers in crypt and villus-like domains show effective barrier function. *Sci Rep* **9**, 1–14 (2019).
31. Pérez-González, C. *et al.* Mechanical compartmentalization of the intestinal organoid enables crypt folding and collective cell migration. *Nat Cell Biol* 1–26 (2021) doi:10.1038/s41556-021-00699-6.
32. Altay, G., Batlle, E., Fernández-Majada, V. & Martínez, E. In vitro Self-organized Mouse Small Intestinal Epithelial Monolayer Protocol. *Bio Protoc* **10**, 1–21 (2020).
33. Cheng, H. & Leblond, C. P. Origin, differentiation and renewal of the four main epithelial cell types in the mouse small intestine V. Unitarian theory of the origin of the four epithelial cell types. *American Journal of Anatomy* **141**, (1974).
34. Parker, A. *et al.* Cell proliferation within small intestinal crypts is the principal driving force for cell migration on villi. *FASEB Journal* **31**, 636–649 (2017).
35. Barriga, F. M. *et al.* Mex3a Marks a Slowly Dividing Subpopulation of Lgr5+ Intestinal Stem Cells. *Cell Stem Cell* **20**, 801-816.e7 (2017).
36. Guillamat, P., Blanch-Mercader, C., Pernollet, G., Kruse, K. & Roux, A. Integer topological defects organize stresses driving tissue morphogenesis. *Nat Mater* **21**, 588–597 (2022).
37. Mao, Q. *et al.* Tension-driven multi-scale self-organisation in human iPSC-derived muscle fibers. *Elife* **11**, e76649 (2022).
38. Eyden, B. The myofibroblast: Phenotypic characterization as a prerequisite to understanding its functions in translational medicine: Translational Medicine. *J Cell Mol Med* **12**, 22–37 (2008).
39. Eyden, B., Curry, A. & Wang, G. Stromal cells in the human gut show ultrastructural features of fibroblasts and smooth muscle cells but not myofibroblasts. *J Cell Mol Med* **15**, 1483–1491 (2011).
40. Powell, D. W., Pinchuk, I. V., Saada, J. I., Chen, X. & Mifflin, R. C. Mesenchymal Cells of the Intestinal Lamina Propria. *Annu Rev Physiol* **73**, 213–237 (2011).
41. Hinz, B., Celetta, G., Tomasek, J. J., Gabbiani, G. & Chaponnier, C. Alpha-smooth muscle actin expression upregulates fibroblast contractile activity. *Mol Biol Cell* **12**, 2730–2741 (2001).
42. Roulis, M. & Flavell, R. A. Fibroblasts and myofibroblasts of the intestinal lamina propria in physiology and disease. *Differentiation* **92**, 116–131 (2016).
43. Sato, T. *et al.* Paneth cells constitute the niche for Lgr5 stem cells in intestinal crypts. *Nature* **469**, 415–418 (2011).
44. McCarthy, N. *et al.* Smooth muscle contributes to the development and function of a layered intestinal stem cell niche. *Dev Cell* **58**, 550-564.e6 (2023).
45. Huycke, T. R. *et al.* Patterning and folding of intestinal villi by active mesenchymal dewetting. doi:10.1101/2023.06.25.546328.
46. Gaggioli, C. *et al.* Fibroblast-led collective invasion of carcinoma cells with differing roles for RhoGTPases in leading and following cells. *Nat Cell Biol* **9**, 1392–1400 (2007).
47. Attieh, Y. *et al.* Cancer-associated fibroblasts lead tumor invasion through integrin-β3-dependent fibronectin asse. *Journal of Cell Biology* **216**, 3509–3520 (2017).
48. Gopal, S. *et al.* Fibronectin-guided migration of carcinoma collectives. *Nat Commun* **8**, 14105 (2017).
49. Pascal, R. R., Kaye, G. I. & Lane, M.D, N. Colonic Pericryptal Fibroblast Sheath: Replication, Migration, and Cytodifferentiation of a Mesenchymal Cell System in Adult Tissue: I. Autoradiographic studies of normal rabbit colon. *Gastroenterology* **54**, 835–851 (1968).
50. Labernadie, A. *et al.* A mechanically active heterotypic E-cadherin/N-cadherin adhesion enables fibroblasts to drive cancer cell invasion. *Nat Cell Biol* **19**, 224–237 (2017).

51. Schaller, V., Weber, C., Semmrich, C., Frey, E. & Bausch, A. R. Polar patterns of driven filaments. *Nature* **467**, 73–7 (2010).
52. Li, X. *et al.* On the mechanism of long-range orientational order of fibroblasts. *Proc Natl Acad Sci U S A* **114**, 8974–8979 (2017).
53. Guillamat, P., Blanch-Mercader, C., Pernollet, G., Kruse, K. & Roux, A. Integer topological defects organize stresses driving tissue morphogenesis. *Nat Mater* **21**, 588–597 (2022).
54. Doostmohammadi, A., Thampi, S. P. & Yeomans, J. M. Defect-Mediated Morphologies in Growing Cell Colonies. *Phys Rev Lett* **117**, 1–5 (2016).
55. Duclos, G., Garcia, S., Yevick, H. G. & Silberzan, P. Perfect nematic order in confined monolayers of spindle-shaped cells. *Soft Matter* **10**, 2346–2353 (2014).
56. Duclos, G., Erlenkämper, C., Joanny, J.-F. & Silberzan, P. Topological defects in confined populations of spindle-shaped cells. *Nat Phys* **13**, 1–6 (2016).
57. Comelles, J. *et al.* Epithelial colonies in vitro elongate through collective effects. *Elife* **10**, e57730 (2021).
58. Farooqui, R. & Fenteany, G. Multiple rows of cells behind an epithelial wound edge extend cryptic lamellipodia to collectively drive cell-sheet movement. *J Cell Sci* **118**, 51–63 (2005).
59. Begnaud, S., Chen, T., Delacour, D., Mège, R. M. & Ladoux, B. Mechanics of epithelial tissues during gap closure. *Curr Opin Cell Biol* **42**, 52–62 (2016).
60. Guillot, C. & Lecuit, T. Mechanics of Epithelial Tissue Homeostasis and Morphogenesis. *Science (1979)* **340**, 1185–1189 (2013).
61. Sonam, S. *et al.* Mechanical stress driven by rigidity sensing governs epithelial stability. *Nat Phys* **19**, 132–141 (2023).
62. Trepat, X. *et al.* Physical forces during collective cell migration. *Nat Phys* **5**, 426–430 (2009).
63. Terzić, J., Grivennikov, S., Karin, E. & Karin, M. Inflammation and Colon Cancer. *Gastroenterology* **138**, 2101-2114.e5 (2010).
64. Karin, M. & Clevers, H. Reparative inflammation takes charge of tissue regeneration. *Nature* **529**, 307–315 (2016).
65. Barker, N. *et al.* Identification of stem cells in small intestine and colon by marker gene Lgr5. *Nature* **449**, 1003–7 (2007).
66. Fernández-Majada, V. *et al.* The tumour suppressor CYLD regulates the p53 DNA damage response. *Nat Commun* **7**, (2016).
67. Yin, X. *et al.* Niche-independent high-purity cultures of Lgr5 + intestinal stem cells and their progeny. *Nat Methods* **11**, 106–112 (2014).
68. Khalil, H., Nie, W., Edwards, R. A. & Yoo, J. Isolation of primary myofibroblasts from mouse and human colon tissue. *Journal of Visualized Experiments* 1–6 (2013) doi:10.3791/50611.
69. Thielicke, W. & Stamhuis, E. J. PIVlab – Towards User-friendly, Affordable and Accurate Digital Particle Image Velocimetry in MATLAB. *J Open Res Softw* **2**, (2014).
70. Püspöki, Z., Storath, M., Sage, D. & Unser, M. Transforms and Operators for Directional Bioimage Analysis: A Survey. in *Focus on Bio-Image Informatics* (ed. Vos, W. H. De) 69–92 (Springer International Publishing Switzerland, 2016). doi:10.1007/978-3-319-28549-8_3.
71. Gregorieff, A. *et al.* Expression Pattern of Wnt Signaling Components in the Adult Intestine. *Gastroenterology* **129**, 626–638 (2005).